

Nip in the Bud: Forecasting and Interpreting Post-exploitation Attacks in Real-time through Cyber Threat Intelligence Reports

Tiantian Zhu, Jie Ying, Tieming Chen*, Chunlin Xiong, Wenrui Cheng, Qixuan Yuan, Aohan Zheng, Mingqi Lv, Yan Chen, *Fellow, IEEE*

Abstract—Advanced Persistent Threat (APT) attacks have caused significant damage worldwide. Various Endpoint Detection and Response (EDR) systems are deployed by enterprises to fight against potential threats. However, EDR suffers from high false positives. In order not to affect normal operations, analysts need to investigate and filter detection results before taking countermeasures, in which heavy manual labor and alarm fatigue cause analysts miss optimal response time, thereby leading to information leakage and destruction. Therefore, we propose Endpoint Forecasting and Interpreting (EFI), a real-time attack forecast and interpretation system, which can automatically predict next move during post-exploitation and explain it in technique-level, then dispatch strategies to EDR for advance reinforcement. First, we use Cyber Threat Intelligence (CTI) reports to extract the attack scene graph (ASG) that can be mapped to low-level system logs to strengthen attack samples. Second, we build a serialized graph forecast model, which is combined with the attack provenance graph (APG) provided by EDR to generate an attack forecast graph (AFG) to predict the next move. Finally, we utilize the attack template graph (ATG) and *graph alignment plus algorithm* for technique-level interpretation to automatically dispatch strategies for EDR to reinforce system in advance. EFI can avoid the impact of existing EDR false positives, and can reduce the attack surface of system without affecting the normal operations. We collect a total of 3,484 CTI reports, generate 1,429 ASGs, label 8,000 sentences, tag 10,451 entities, and construct 256 ATGs. Experimental results on both DARPA Engagement and large scale CTI dataset show that the alignment score between the AFG predicted by EFI and the real attack graph is able to exceed 0.8, the forecast and interpretation precision of EFI can reach 91.8%.

Index Terms—Real-time Threat Prediction, Attack Detection, Attack Interpretation, Advanced Persistent Threat, CTI Report

1 INTRODUCTION

With the rapid development of the Internet, APT attacks have been frequently occurred around the world. According to a report released by CSIS [1] in August 2023, there have been more than 7,000 significant APT attacks on governments, defense departments, and high-tech companies since 2006.

To combat possible APT attacks in the endpoint, EDR systems are deployed by enterprises to block malicious behaviors and provide suggestions for system repair. Audit logs (e.g., ETW for Windows [2], and Audit for Linux [3]) are

often collected by EDR to observe the interaction behavior between system entities so as to search for traces of the attackers. However, due to the high persistence of APT attacks [4], endpoints will generate an enormous volume of system logs during the collection process, and majority of these logs result from normal applications [5]. To find an attack is like looking for a needle in a haystack. In addition, some normal applications will perform like “suspicious behavior” (e.g., a newly installed benign browser may trigger six tactics in the ATT&CK model [6] and raise an alarm [7]), which drowns true alarms in false positives. In real enterprise scenarios, response methods require human intervention limited by high false positive rate of detection (automated responses have a high probability of killing benign programs, which will undoubtedly affect normal operations). Therefore, it is arduous to reduce Mean-time-to-response (MTTR), which is one of the most crucial metrics for the defense: CrowStrike reports that the average lateral movement time for APT attacks is 1h 58mins [8], which means that enterprises must complete a series of initiatives (e.g., detection, investigation, and response) within two hours to prevent information leakage or destruction.

We try to solve the above problems from a new perspective: Nip in the Bud. If we can get one step ahead of the attacker, automatically predict next move during post-exploitation, interpret the forecasting results in technique-level and dispatch the strategy to EDR for advance reinforcement, the above dilemmas will be addressed. By

- This work is supported in part by the following grants: National Natural Science Foundation of China under Grant No. 62002324, U22B2028 and U1936215. Fuxi Foundation of CCF-SANGFOR under Grant No. 20220201. Zhejiang Provincial Natural Science Foundation of China under Grant No. LQ21F020016 and LY20F020027. Key R&D Projects in Zhejiang Province under Grant No. 2021C01117. “Ten Thousand People Program” Technology Innovation Leading Talent Project in Zhejiang Province under Grant No. 2020R52011; Major Program of Natural Science Foundation of Zhejiang Province under Grant No. LD22F020002.
- T. Zhu, J. Ying, T. Chen*, W. Cheng, Q. Yuan, A. Zheng and M. Lv are with the College of Computer Science and Technology, Zhejiang University of Technology, Hangzhou 310023, China. E-mail: ttzhu@zjut.edu.cn, jieying@zjut.edu.cn, tmchen@zjut.edu.cn, zjutcwr@zjut.edu.cn, zjutyqx@zjut.edu.cn, zhengaohan198@163.com, mingqilv@zjut.edu.cn. *corresponding author
- C. Xiong is with Department of Shenzhen Institutes of Advanced Technology, Chinese Academy of Sciences, Shenzhen 518052, China. E-mail: xiongchunlin@sangfor.com.cn.
- Y. Chen is with Department of Electrical Engineering and Computer Science, Northwestern University, Evanston, IL 60208, USA. E-mail: ychen@northwestern.edu.

analyzing literature related to APT in the past five years, we find that: First, analysts often use the provenance graph in EDR to describe the activities of the attacker. Second, statistical-based and policy-based provenance graph analysis [5, 9–11] requires heavy manual labor and lacks generalization ability, while learning-based methods [12–14] often face the problem of a scarcity of attack samples. Third, CTI reports written by professional security analysts incorporate knowledge of attack scenarios, TTPs of ATT&CK model [6], Indicators of Compromise (IOC), and their causal relationships, which provides detailed information on cyber attacks. Based on the above observations, in this paper, we attempt a best practice: strengthen attack (graph) samples with the help of CTI reports, and construct a learning-based model for post-exploitation attack forecast and interpretation. We summarize main challenges as follows:

I: How to deal with the lack of samples in APT attack analysis? Since the high complexity of APT attacks, it is time-consuming to simulate different attack techniques on real systems and collect corresponding logs.

II: How to bridge the semantic gap between CTI reports described by natural language (high-level) and system logs (low-level)? Current studies [15–17] have difficulty (e.g., the association of contextual semantics, the transformation of multi-hop equivalent semantic, and the extraction of dependency attributes) in automating the extraction of accurate ASG composed of entities and dependencies (events) with extremely different writing styles.

III: How to proactively and accurately predict post-exploitation attacks in real-time? The judgment of the attacker's next move is overly depending on the experienced knowledge of security analysts, and the variety of attack techniques can make the decision-making difficult.

IV: How to interpret the attack in technique-level based on the forecasting results? In most cases, the attack forecasting results generated by learning-based models lack explanation in technique-level. Even with expertise, analysts are hard to directly use the forecasting results (graphs) to take counter-measures.

To tackle the aforementioned challenges, we propose and open source EFI¹, a real-time attack forecast and interpretation system. In summary, we make the following contributions:

- To the best of our knowledge, we are the first to work on automated forecasting and interpreting post-exploitation attacks on endpoints in real-time, which can avoid the impact of existing EDR false positives, and tremendously reduce the attack surface of system without affecting the normal operations.
- For Challenges I and II, we build an ASG extraction module to achieve massive abstraction of ASGs (can be mapped to system-level logs to bridge the semantic gap) from CTI reports by adopting heuristic natural language processing (NLP) pipeline.
- For Challenge III, we construct an AFG generation module with the help of a serialized graph

forecast model for realizing the sub-graph prediction. This module simultaneously captures node attributes, edge attributes, and edge time ordering of the graph to maximize the forecasting fidelity of post-exploitation attacks.

- For Challenge IV, we construct ATGs based on the atomic red team technique [18], and incorporate an innovative *graph alignment plus algorithm* to provide further interpretability for AFG, which facilitates automation to graph investigation for EDR to implement advance reinforcement.
- We conduct a detailed evaluation of all the modules in EFI. The results show that EFI can generate an AFG within 5s, interpret the AFG in technique-level within 5mins and obtain an alignment score of more than 0.8, the forecast and interpretation precision of EFI can reach 91.8%.

2 MOTIVATION AND BACKGROUND

2.1 Motivating Example

We assume there is a real-world campaign that the group APT28 [19] is trying to compromise the enterprise system to steal confidential data. Refer to a known set of tactics and techniques that APT28 commonly use listed by MITRE [20]. The attacker of APT28 induces the victim to download malware, then executes the malicious file, collects the target data, and finally steals confidential data over C2 Channel. Meanwhile, an employee downloads and installs the firefox browser locally, and then firefox collects local data for configuration.

Limitations of EDR tools: Existing EDR tools have a high rate of false positives, the two examples have great similarity in procedure and both hit the rule based alert condition "download & execution" [5, 7, 21–23]. While for anomaly based methods [12, 13], the aforementioned situation becomes even more challenging to distinguish. More specifically, assuming that *ABCD* represents a sequence of actions performed by a legitimate program, and *ABCX* represents a sequence of actions carried out by an attacker. Although detecting the presence of sensitive behavior in the system solely based on *ABC* can trigger an alert from EDR, it is not sufficient to determine whether an attack is taking place (i.e., further analysis is needed to determine if action *D* or *X* follows). By the time the alert is triggered after the attacker has completed *ABCX*, it is already too late for EDR to response as the damage has already occurred. To avoid the **choice dilemma** (i.e., to kill or not to kill when alerts like *ABC* are triggered), it is necessary for analysts to proactively forecast the attacker's next move in real-time and carry out targeted defensive measures before the ultimate goal is achieved during post-exploitation.

Therefore, we propose EFI as a third-party tool for existing EDRs, capable of forecasting next move during post-exploitation, explaining attacks in technique-level and dispatching strategies to EDR for advance reinforcement. **After reinforcement, we consider two status:** 1) There exists a false alarm and the process does not perform any suspicious actions (i.e., *D*), then the restriction can be removed heuristically (e.g., exceeding average lateral movement time [8]). 2) If the process performs the predicted operation (i.e.,

1. <https://github.com/EFI-Demo/Endpoint-Forecasting-and-Interpreting>

X), the EDR will block the event, raise a high-level alarm and notify the analyst. Since the corresponding point has been reinforced in advance, the attacker will not achieve his goal. **It is important to note that in order to ensure the accuracy of the forecast results, the EDR can automatically verify whether the predicted event, combined with the existing behavior, satisfies a complete context of an attack (i.e., graph investigation). If it does, EDR systems will directly block the corresponding predicted event** (also mentioned in Section 4.4).

2.2 Causal Graph and Heterogeneous Graph

Causal graph is a data structure extracted from low-level system logs representing causal relationships (e.g., exec, read, etc.) between subjects (e.g., processes) and objects (e.g., files). We here consider a directed causal graph whose edges point from a subject to an object.

Heterogeneous graph is defined as $G = (V, E)$, the set of nodes is $V = (v_1, \dots, v_n)$ and the set of edges between nodes is $E = (v_i, v_j | v_i, v_j \in V)$, where each node and edge corresponds to a specific attribute. Denoting the set of node attributes by Γ_v and the set of edge attributes by Γ_e , the heterogeneous graph requires $|\Gamma_v| + |\Gamma_e| > 2$. Obviously, causal graph is a kind of heterogeneous graph, and all the graph structures mentioned in this paper are heterogeneous graphs.

3 OVERVIEW

3.1 Graph Description

In this paper, we divide attack graphs into four categories as follows: **Attack scene graph (ASG)** is automatically extracted from CTI reports for training graph forecast model. It can be mapped to low-level system logs to strengthen attack samples. **Attack provenance graph (APG)** is a potential attack chain extracted by EDR based on alarm point through forensic analysis from low-level system logs and used for subsequent post-exploitation attacks forecasting. **Attack forecast graph (AFG)** is generated by the graph forecast model, which contains the initial APG and next operation(s) of potential attackers. **Attack template graph (ATG)** is a technique template that we construct from atomic red team [18] for interpreting AFG.

3.2 Threat Model

In this paper, we consider a complex enterprise environment. We assume that the enterprise has deployed a mature EDR system with massive false positives (a common problem of EDR in the industry). The enterprise has high requirements for the stability of its production environment and cannot directly kill all processes related to alarms. Next, we assume that the APT attack occurs after the EDR is deployed, the EDR can issue alarms without being compromised, and provide the APG of the alarm in real-time (e.g., the method proposed by [10]). Finally, we do not consider attack methods that cannot be detected by EDRs, such as hardware Trojans, side channels, and backdoors.

TABLE 1

The attribute of system entities in EFI. The second column indicates the symbol of entity attribute in the system.

Entity	Symbols	Description
File	F0	Sensitive files such as '/etc/passwd'.
	F1	Library files such as '*.dll', '*.so'.
	F2	Executable files such as '*.exe', '*.vbs'.
	F3	Other files.
	FR	Registry files such as 'HKCR', 'HKLM'
Process	P	Such as PID, user, group.
Socket	S	Such as IP, Domain.

3.3 Our Approach

The architecture of EFI is shown in Figure 1. First, EFI automates the extraction of ASGs (contain entities and events that can be mapped to low-level system logs) from unstructured CTI reports without human intervention. Figure 5 gives an example of ASG from the Darpa Engagement CTI report. The attributes of system entities and events are shown in Table 1 and Table 2, respectively. The reason we divide file entities into four attributes is that different file types imply different purposes of attackers. Fine-grained division can also effectively reduce false positives of subsequent AFG interpretations.

Then, EFI uses ASGs to train a serialized graph forecast model that maximally learns the graph distribution. In addition, EFI also performs targeted optimization of the graph forecast model to capture the node attributes, edge attributes and edge time ordering of the graph at the same time. The trained model takes the APG (provided by the deployed EDR system) as input to serially forecasts: 1) the attribute of the next node, and 2) the dependency between the new node and all the existing nodes (whether there is an edge and the type of the specific edge), to finally obtain the AFG.

Besides, we construct ATGs based on the atomic red team technique [18] to interpret the AFG (Details of ATGs are shown in Section 5.3 and Appendix A, and we open source ATGs). We propose the *graph alignment plus algorithm* to calculate the similarity between the AFG and different ATGs, and use the ATGs exceeding the threshold as the technical explanation of AFG.

Finally, EFI will combine the interpretation results and technique-level attack detection/investigation tools (e.g., APTSHIELD [24]) to dispatch strategies to EDR for advance reinforcement, thus avoiding the impact of EDR false positives and being able to reduce the attack surface of the system without affecting the normal operations. It is important to note that whether it is the ASG, AFG, APG or ATG, **EFI only retains its node attributes and discards the node names**. This is because the latter is susceptible to dynamic changes by attackers and EFI prefers to learn the graph distribution representing the attack procedure.

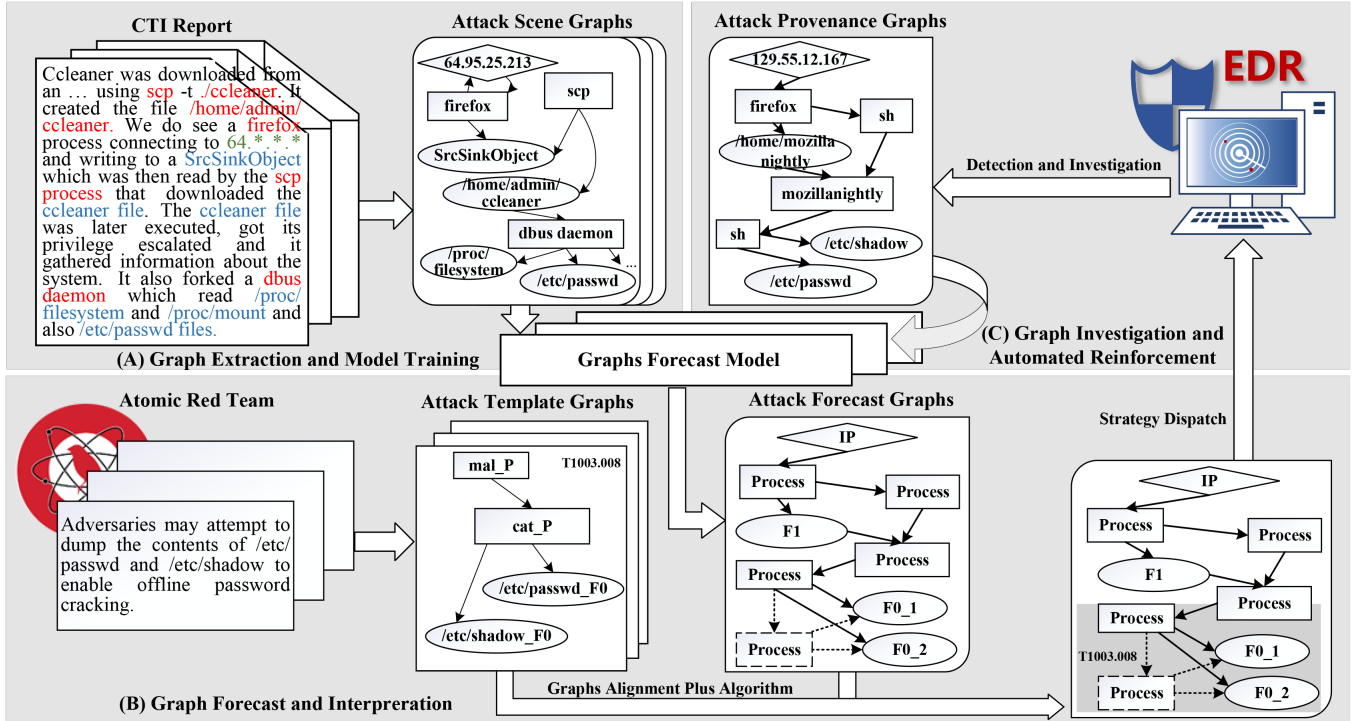


Fig. 1. The architecture of EFI. EFI extracts ASGs from open source CTI reports and trains the graph forecast model. The APG provided by EDR is then fed into the model to predict the AFG, which is then interpreted using the *graph alignment plus algorithm* and ATGs. Finally, the interpretation results are used to dispatch strategies to EDR for advance reinforcement.

TABLE 2

The attribute of system events in EFI. P indicates process, F indicates file, and S indicates socket in column 2.

Type	Sub.	Obj.	Description
Write	P	F	A process writes a file.
Execute	P	F	A process executes a file
Read	F	P	A file is read by a process.
Send	P	S	A process sends information to a socket.
Receive	S	P	Information from a socket is received by a process.
Fork/Clone	P	P	A process starts a new process.

4 SYSTEM DESIGN

4.1 ASG Extraction

In this section, we present the details about extracting ASGs that can be mapped to the low-level system logs from unstructured CTI reports. A useful CTI report would provide an exhaustive chronological description of the attacker's actions on the victim host. Normally, these descriptions include the involved entities as well as their interactions. To extract the ASGs, it is imperative to bridge the huge semantic gap between unstructured CTI and low-level system logs. We summarize several challenges as follows:

C1 Text Verbosity. In general, CTI reports are redundant. Sentences that related to the attack are often drowned out in the tedious text. For example, only 9 sentences describe the attack out of more than 300 lines of reports on Flamer [25].

C2 Related Entity Recognition. We divide attack-related entities into IOC and non-IIOC entities in CTI reports. IOC entities refer to domain-specific terms, including IP addresses, paths, and registries. Non-IIOC entities are compo-

nents that represent important entities by various expressions (e.g., using a group name for a subject to describe an attack scenario), which can cause semantic deficiencies or confusion in the ASG if they are not properly recognized. Besides, it is essential to address the ubiquity problem of reference, which is classified as anaphora and co-reference. To illustrate, "it" and "the user" are both used to represent Host A, as shown in the text of Figure 5.

C3 Dependency Extraction. To properly construct the ASG, we need to extract relationships between different attack entities. However, even for the same attack, different analysts produce heterogeneous CTI reports (using different phrases, verbs, structures). This will result in inaccurate extraction of dependencies.

To address the above challenges, We design a customized NLP pipeline to correctly identify entities, extract dependencies and construct ASGs as follows:

Step 1: Verbosity filtering. We use sentence tokenizer to divide the text into sentences, and then employ the self-trained verbosity filtering model to filter the attack irrelevant sentences. We then retrained the BERT model [26] to filter the irrelevant texts. The training process, parameters and the performance of model are in Section 5.1 and Section 6. (C1)

Step 2: Attack-related entities identification and protection. Inspired by [27–29], we construct a new BERT-BiLSTM-CRF model for attack-related entity type recognition (first column 'Entity' in Table 1). The BERT model [26] can enhance the semantic representation of sentences, while the bidirectional LSTM network (BiLSTM) [30] can automatically learns the intrinsic connections in the sentence context, and the Conditional Random Field (CRF) [31] can restrict the

syntax and ensure the plausibility of the predicted labels in terms of order. Then, we combine regular expressions [16] to subdivide entity attributes (second column 'Symbols' in Table 1) and replace entities with them to protect the IOC from being mishandled by the NLP modules. (C2)

Step 3: Anaphora resolution. We use a popular pronoun resolution model, NeuralCoref [32], to map and replace pronouns (e.g., it/that) with previously mentioned entities they refer to. (C2)

Step 4: Dependency Extraction. After reading a large number of CTI reports, we summarized the types of events necessary to construct an ASG, as shown in Table 2. In order to extract dependencies correctly from CTI reports, the key insight we rely on is that the types of subject-object pair for different events are distinctive, e.g., Write: P → F, Receive: S → P, with the exception of "Read" and "Execute" events (both of which are F → P). In other words, **after identifying the types of attack-related entity pairs and the interaction direction, we can determine dependencies directly**. Thus, for all attack-related entities in each sentence, we combine them in pairs (discarding impossible entity pairs, e.g., F → F), and identify the subject and object in these entity pairs (determine the interaction direction) by using part-of-speech (POS) annotation [33] and dependency tree [34]. In addition, for events ("Read" and "Execute") where the subject is of type F and the object is of type P, we vectorize them [35] to calculate the Euclidean distance separately, and then choose the smaller one as the dependency type. By adopting the above mechanism, we construct multiple triples <sub, verb, obj>. (C3)

Step 5: Co-reference Resolution. Even if entities in different triples are the same, there will be differences in names due to human descriptions. For each entity N, we iteratively calculate the similarity score between N and the entities from other triples. We rename N when the similarity score exceeds the threshold. We consider the differences in naming N_{name} between entities, the index N_{index} of the triple where the entity is located, and the type N_{type} between entities, where W_d and W_t are preset weights. The similarity score between entity N and M is calculated as follows: (C2)

$$Sim(N, M) = \text{sim}(N_{name}, M_{name}) - \frac{|N_{index} - M_{index}|}{W_d} - \frac{|N_{type} - M_{type}|}{W_t} \quad (1)$$

4.2 AFG Forecast

In this section, we primarily focus on how to use APGs to generate AFGs.

Goal and Challenge. The goal of this module is to learn the distribution $p_{model}(G)$ of extracted ASGs $\mathbb{G} = \{G_1, \dots, G_s\}$, and use the learned distribution to generate graph structure with a certain number of steps for arbitrarily structured graph inputs, thus enabling the generation of AFG. Inspired by You et al.'s work on GraphRNN [36], we generate AFGs serially with a deep auto-regressive model. However, we meet several challenges. First, GraphRNN only considers homogeneous graphs, but for heterogeneous graphs, the node and edge attributes are crucial for the graph structure generation (e.g., there is no direct interaction between two file entities in the system). Second, it is difficult for GraphRNN to solve the non-convergence problem caused by the sparsity of the adjacency matrix

during training (e.g., there are only 200 available values in a 40x40 adjacency matrix). For these challenges, we extend the usage of GraphRNN model to heterogeneous graphs and combine the average number of nodes in technique templates (see Section 5 for details) to shrink the matrix for sparsity mitigation.

Definition and Methodology. The attack graphs in this paper are specifically defined as $G = (V, E)$, where the set of nodes is $V = (v_1, \dots, v_n)$, and the set of edges between nodes is $E = (v_i, v_j | v_i, v_j \in V)$. According to certain order of nodes π , the graph can be represented in the form of adjacency matrix $A^\pi \in \{S_{i,j}^\pi\}^{n \times n}$. To illustrate, π is a substitution function on V (i.e., $(\pi(v_1), \dots, \pi(v_n))$), the adjacency element $S_{i,j}^\pi \in \{0, 1, 2, \dots, P\}$ denotes the interaction type between system entities, and the adjacency vector $S_i^\pi = (S_{1,i}^\pi, \dots, S_{i-1,i}^\pi)^T$ denotes the interaction between node $\pi(v_i)$ and the previous nodes in π order. Moreover, the node type $C_i^\pi \in \{0, 1, 2, \dots, K\}$ indicates that the node belongs to a certain entity attribute, and the list of all nodes is $C^\pi = (C_1^\pi, \dots, C_n^\pi)$.

In order to generate graph structures serially, it is crucial to represent graphs with different node orderings as sequences and then build auto-regressive generative models on these sequences. Therefore, we first define a mapping function f_S to map graphs to sequences:

$$p(S^\pi, C^\pi) = f_S(G, \pi) = ((S_1^\pi, C_1^\pi), \dots, (S_n^\pi, C_n^\pi)) \quad (2)$$

Where $G \in \mathbb{G}$, G contains n nodes and is represented by the order of nodes π . At this point, the graph G can be represented by a fixed sequence S^π and C^π , and the distribution $p(G)$ that we want to learn on the graph can be represented as $p(S^\pi, C^\pi)$. Because of the serial property of π , we can split it into the following likelihood function:

$$p(S^\pi, C^\pi) = \prod_{i=1}^{n+1} p(C_i^\pi | S_{<i}^\pi, C_{<i}^\pi) p(S_i^\pi | C_i^\pi, S_{<i}^\pi, C_{<i}^\pi) \quad (3)$$

First, the graph information consisting of the preceding $i-1$ nodes is utilized to predict the attribute of the new node. Subsequently, the information from the original graph with $i-1$ nodes and the predicted node are merged together to forecast the dependence between the predicted node and its predecessor. Note that for the termination node $n+1$, $p(C_{n+1}^\pi | S_{<n+1}^\pi, C_{<n+1}^\pi) \equiv 1$.

We refer to the function that predicts the type of a new node as NodeRNN and the function that predicts the dependency between a new node and its predecessor as EdgeRNN. In our model, once the information of the previous $i-1$ nodes under the node order π is determined (i.e., the subgraph/APG is determined), NodeRNN is able to determine the next node i 's node type C_i^π . And based on the graph information composed of the previous $i-1$ nodes and the output of NodeRNN h_i^{node} , the model EdgeRNN is able to generate the dependency relationship between node i and its predecessor node (i.e., the adjacency vector S_i^π). The structure of the whole graph forecast model is shown in Figure 2, the specific parameter settings are shown in Section 5.2, and the specific formulas are as follows:

$$\begin{aligned} \text{input}_{i-1} &= \text{concat}[\text{emb}(S_{i-1}^\pi), \text{emb}(C_{i-1}^\pi)] \\ h_i^{node}, C_i^\pi &= \text{NodeRNN}(h_{i-1}^{node}, \text{input}_{i-1}), \quad h_0^{node} = 0 \\ h_{i,j}^{edge}, S_i^\pi &= \text{EdgeRNN}(h_{i,j-1}^{edge}, \text{emb}(S_{i,j-1}^\pi)), \quad h_{i,0}^{edge} = h_i^{node} \end{aligned} \quad (4)$$

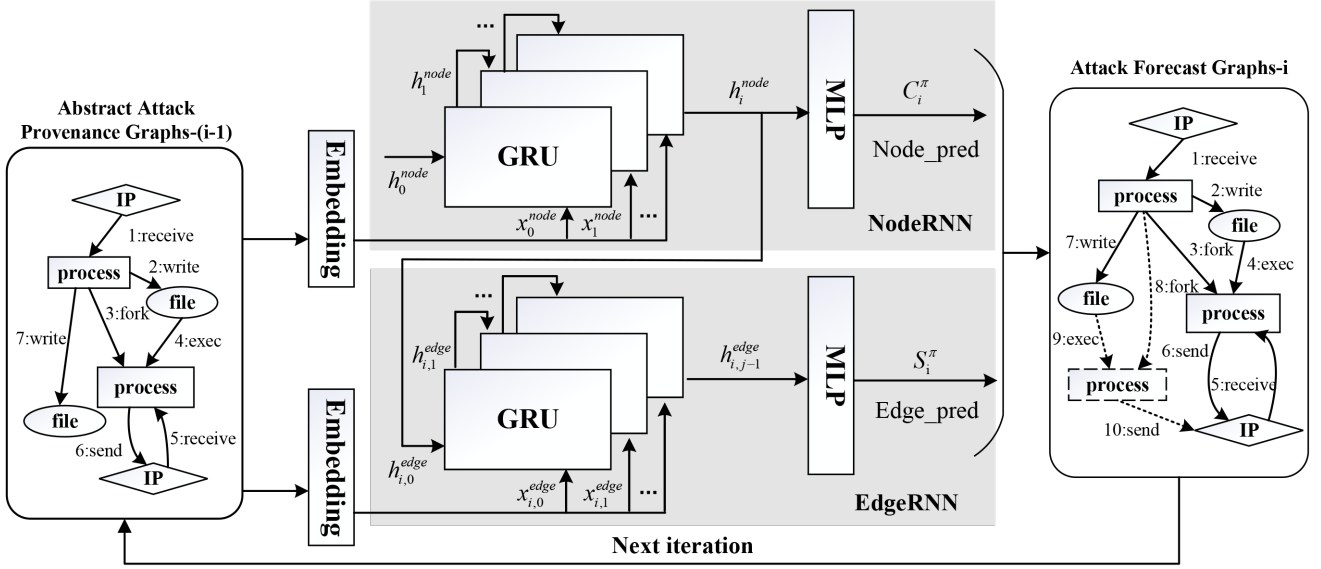


Fig. 2. Graph Forecast Model Architecture. The current forecast results can be used as input for the next round of prediction for serialized graph generation.

Where concat refers to the stitching between tensors. Since the attack graph is chronological (all system events occur in a backward and forward order in low-level system logs), the node order π of the attack graph is determined.

4.3 AFG Interpretation

In this section, we first introduce how to construct ATGs. Then, we use ATGs to interpret AFGs at the attack technique-level (i.e., determine whether the ATG exists in the AFG). Inspired by the graph alignment algorithm in Poirot [37], we redesigned and improved the algorithm by proposing *graph alignment plus algorithm*, which extends the algorithm to the abstract level to compute the alignment score in terms of node attributes, edge attributes, and graph structure, while considers the **Multi-Hop Equivalent Semantics (MHES)** problem, which is common in attacks.

ATG construction: Atomic red team [18] is a test library proposed by Red Canary that can be mapped to MITRE ATT&CK. It contains descriptions and implementations of different attack techniques (atomic tests, currently 265 in total). By reviewing these, we manually construct the ATG for each atomic test, as shown in Appendix A. ATGs reflect the form of low-level system log of the attack techniques with multiple nodes and edges, where nodes represent entities and edges indicate events. And the relevant statistical data about ATGs are shown later in Section 5.3.

Graph alignment plus algorithm: We mainly calculate the alignment score $\Gamma(G_q : G_p)$ by applying the graph alignment plus algorithm to quantitatively determine the presence of the ATG (G_q) in the AFG (G_p). And the implementation of the algorithm can be summarized in three steps: 1) Find candidate nodes. Find all corresponding candidate nodes k in G_p for all nodes i in G_q , respectively, and we call the set of candidate nodes corresponding to i as $\Gamma_C(i)$. 2) Fix candidate nodes. Iterate through the node scores of all candidate nodes of node i , select the node m with the highest score and greater than the threshold value

as the fixed node of node i ($m \in \Gamma_C(i)$), we note the fixed node corresponding to i as $\Gamma_F(i)$. 3) Compute the graph alignment score. After determining the fixed nodes of all nodes in G_q , we compute the alignment score $\Gamma(G_p, G_q)$ between two graphs.

The method for determining candidate nodes is shown in Equation 5, and if $Candi(i : k)$ is 1 then k is added to $\Gamma_C(i)$, where i_{degree} denotes the degree of node i . The node score of the candidate node is calculated as shown in Equation 6, where $(i \Rightarrow j)$ denotes the path starting with i and ending with j , both i and k are fixed as inputs. The path score is calculated as shown in Equation 7, where i', j' is the node in path $i \Rightarrow j$, $i' \rightarrow j'$ is an edge formed by i', j' , and $(i' \rightarrow j')$ is an edge in path $i \Rightarrow j$. The edge score is calculated as shown in Equation 8, where judgment conditions of MHES will be introduced later. Finally, the graph alignment score $\Gamma(G_q, G_p)$ is computed as shown in Equation 9, which represents a quantitative determination of the presence of G_q in G_p .

$$Candi(i : k) = \begin{cases} 1, & i_{type} = k_{type} \wedge i_{degree} \leq k_{degree} \\ 0, & \text{else} \end{cases} \quad (5)$$

$$NodeScore(i, k) = \sum_{j \in G_q} \frac{PathScore(i, j : k)}{(i \Rightarrow j)} \quad (6)$$

$$PathScore(i, j : k) = \sum_{\substack{i', j' \in i \Rightarrow j \\ i' \rightarrow j' \in i \Rightarrow j}} \frac{EdgeScore(i', j' : k)}{(i' \rightarrow j')} \quad (7)$$

$$EdgeScore(i', j' : k) = \sum_{\substack{l \in \Gamma_C^j \\ k, l \in G_p}} \frac{MHES(i', j' : k, l)}{(k \Rightarrow l)} \quad (8)$$

$$MHES(i', j' : k, l) = \begin{cases} 1, & i' \rightarrow j' \text{ and } k \Rightarrow j \text{ with} \\ & \text{Equivalent Semantics} \\ 0, & \text{else} \end{cases}$$

$$\Gamma(G_p : G_q) = \sum_{i, j \in G_q} \frac{(\Gamma_F(i) \Rightarrow \Gamma_F(j))}{(i \Rightarrow j)} \quad (9)$$

We find that ATG is usually streamlined due to its atomic

TABLE 3
Suspicious Semantic Delivery Rules.

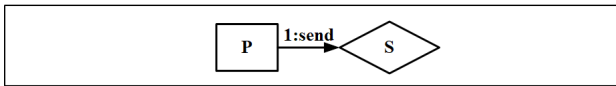
Event Type	Subject	Object	Description
Read	Process	File	The process reads a file containing suspicious semantics and the process is considered to be associated with the attack.
Write	Process	File	A process associated with the attack writes a file, and the file being written contains suspicious semantics.
Load	Process	File	The process that loaded files containing suspicious semantics are considered to be associated with an attack.
Receive	Process	Socket	The process is considered to be associated with the attack after accepting data from the suspicious network.
Send	Process	Socket	The process associated with the attack sends data outward.
Fork/Clone	Process	Process	The process spawns a new process through the Fork/Clone operation and passes suspicious semantics to the new process.

characteristics. If it is directly applied to graph alignment for interpretation, there will be a high number of false negatives. Also, it will be easily avoided by “take a long way” attackers. Fortunately, suspicious semantics of entities will be passed through control flow and information flow [4, 10]. As shown in Figure 3, the suspicious semantics of process P1 in Figure 3(b) will pass to P3 with control flow ($t = 1$) and information flow ($t = 2, 3$), then the semantics of this multi-hop path should be equivalent to the single-hop in Figure 3(a), which represents the proposed concept of MHES.

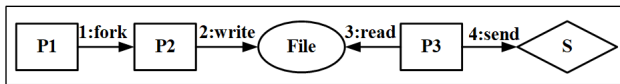
To determine whether there is semantic equivalence between a single-hop edge $i \rightarrow j$ and a multi-hop path $k \rightarrow l$, we summarize the suspicious semantic delivery rules through observing the delivery phenomenon of semantic caused by system entities when passing information flows and control flows, as shown Table 3. We define single-hop edges as $i \rightarrow j = (< v_i, v_j, e_v >)$, n -hop paths as $k \rightarrow l = (< v_1, v_2, e_1 >, < v_2, v_3, e_2 >, \dots, < v_{n-1}, v_n, e_n >)$, expressing the edge information in terms of triples $< subject, object, eventtype >$, with the table of suspicious semantic delivery rules defined as the set U . Then, if

$$\begin{aligned} \exists i.type == v_1.type \wedge j.type == v_n.type \\ \wedge e_v == e_n \wedge < v_{t-1}, v_t, e_t > \in U, \forall t \in [1, n] \end{aligned} \quad (10)$$

We consider the edge $i \rightarrow j$ and the multi-hop path $k \rightarrow l$ are semantic equivalent, and the MHES judgment function in Equation 8 returns 1.



(a) One-hop Edge



(b) Multi-hop Edge

Fig. 3. An example of Multi-Hop Equivalent Semantics.

After calculating the alignment scores of all the technique templates, we compare them with the predefined threshold T and consider that the technique templates G_t exceeding the threshold exist in the AFG G_f , achieving the interpretation of AFG at the technique-level.

4.4 Strategy Dispatch

Graph Investigation. In practical usage, deviations in the prediction results may lead to the blocking of normal behavior. To address this problem, EFI will analyze AFGs by adopting existing attack detection/investigation systems. Here, we can utilize the TTP-based context analysis model proposed in APTSHIELD [24] to examine the integrity and rationality of the AFG (i.e., technique-level analysis), and only AFGs that align with the complete attack flow will be blocked at forecast points. This approach maximizes the value of traditional APT detection systems and transforms their response capabilities into enhanced predictive reinforcement capabilities. Furthermore, we can integrate multiple real-time models (e.g., TTP-based [24], anomaly-based [13], classification-based [14]) to inspect whether AFG constitutes a comprehensive attack, thereby minimizing FPs of forecast results to the greatest extent possible.

Automated Reinforcement. Based on the generation of AFG, EFI will dispatch strategy to EDR, such as predicting $<P, \text{read}, F0>$ to prohibit the process from reading sensitive files (combined with whitelisting), and predicting $<P, \text{send}, S>$ to prohibit the process from communicating with sockets. In addition, these strategies can be combined with heuristic decay, i.e., lifting the restriction after a certain period of time.

5 IMPLEMENTATION

In this section, we will briefly describe the implementation details and the dependent tools in our system. We deployed EFI on a Windows system with Intel (R) Core (TM) i9-10900K CPU @ 3.70GHz and 64GB memory.

5.1 ASG Extraction

We used NLTK [38] for sentence splitting, spaCy [39] for POS annotation and dependency tree construction, NeuralCoref [32] for resolving anaphora. We subsequently optimized models to filter the irrelevant texts and identify the attack-related entities. Specifically, we manually labeled 8,000 sentences and tagged 10,451 entities from blogs of 5 security vendors (bitdefender [40], Microsoft [41], symantec [42], talosintelligence [43], and virustotal [44]). For the methodology of sentence labeling, we followed the purpose of text classification to label them under two classes

TABLE 4

The detailed statistics about the labeled sentence dataset and the tagged entity dataset.

Data Type	Data Label	Count	Ratio(%)
Sentence	Attack-Relevant	4000	50
	Attack-Irrelevant	4000	50
	Total	8000	100
Entity	File	3159	30.2
	Process	4845	46.4
	Socket	2447	23.4
	Total	10451	100

of attack-relevant (label=1) and attack-irrelevant (label=0). For the methodology of entity tagging, we used the BIO scheme [45], where the B-prefix indicates the beginning of the tag, and the I-prefix indicates the inside of the tag. An outside (O) tag is a token indicating that it is not in a predefined category. More detailed statistics on the dataset are presented in Table 4.

We then used the sentences to train the BERT model for redundancy filtering. Besides, we also used the entities to train the BERT-BiLSTM-CRF model for attack-related entity identification. The detailed evaluation is shown in Section 6.3 and Section 6.4. Finally, we used graphviz [46] to visualize the triples and networkX [47] to save the adjacency matrix with more than 5 nodes (we consider that a basic information collection and leakage involves at least 5 nodes), and finally collected 1,429 attack scene graphs, containing a total of 19,212 entities and 27,586 inter-entity dependencies.

5.2 AFG Forecast

We constructed two sub-models, namely NodeRNN and EdgeRNN. In NodeRNN, the adjacency matrix and attributes of predecessor nodes served as the input, which underwent embedding layers and expanded into 64 and 256 dimensional outputs, respectively. Then outputs were concatenated and fed into the GRU network with 4 hidden layers and 128 dimensions. The resulting output h_{output}^{node} was deployed as input for the EdgeRNN and node attribute prediction. Subsequently, EdgeRNN accepted h_{output}^{node} as input and expanded it into 32 dimensions via the embedding layer before inputting it into the GRU network with 4 hidden layers and 64 dimensions. Finally, linear layers transformed the output h_{output}^{edge} to obtain predictions of the edge relationship between node i and its predecessor nodes. In addition, the experiments were conducted with a batch size of 16 and for 50 epochs, while the dataset (ASGs) was divided into 1,143 for training, and 286 for testing. The detailed evaluation are shown in Section 6.5.

5.3 AFG Interpretation

We used the description of the techniques and actual code examples by the atomic red team [18] to build ATGs manually. We ended up with a total of 256 ATGs for each of the available atomic techniques. In total, 882 process nodes, 361 file nodes, 52 registry nodes, 37 socket nodes and 1,192 inter-node dependencies were involved, covering 12 tactics, 123 techniques and 256 sub-techniques, with an average of 5.2 nodes and 4.7 edges per ATG. Finally, ATGs and *graph alignment plus algorithm* are combined to be used for the interpretation of APGs.

6 EVALUATION

In this section, we evaluate the effectiveness of each component of EFI and answer the following four questions.

RQ1: How to prove the effectiveness of EFI on ATG construction?

RQ2: How to prove the effectiveness of graph alignment plus algorithm?

RQ3: How to prove the effectiveness of EFI on ASG extraction?

RQ4: How to prove the effectiveness of EFI on AFG generation?

6.1 Evaluation Preparation

To evaluate EFI, we collected 3,483 open-source CTI reports, extracted a total of 1,429 ASGs, annotated 10,451 attack-related entities and 8,000 sentences, and constructed 256 ATGs. In addition, we performed manual extraction and technique-level interpretation of ASGs on 10 CTI reports, so as to construct ground truth for the evaluation. The above 10 reports were selected to ensure that they cover different operating systems, various kill chains, including 4 from the Darpa Transparent Computing Dataset [48] and 6 from APT organization reports. The specific report names are shown in Table 6, where TC_A1-A4 represent hc attack, ccleaner attack, Information gather and exfiltration, and In-memory attack with firefox in DARPA reports, respectively.

To evaluate the effectiveness of EFI on ASG extraction, we reproduced two latest works EXTRACTOR [16] and AttackG [17] to compare with our system. We selected these two systems due to their similar aims to ours, which involve extracting graphs representing attack behaviors from CTI.

To simulate the role of EDR in real scenarios, as described in Section 3.3, we also reproduced DEPIMPACT [49] for correlated sub-graph investigation of alert point, and reproduced DEPCOMM [50] and CPR [51] for compressing redundant edges and nodes in the sub-graph. We examined the effectiveness of EFI on AFG generation by passing the pruned ASG into the graph forecast model as APG.

In addition, we simulated the cooperation between EFI and EDR tools in the DARPA Engagement dataset (TC_A1-A4) collected under real scenarios as a way to demonstrate that EFI eliminates the gap between CTI reports and the system logs for effective forecast.

6.2 RQ1: How to prove the effectiveness of ATG construction?

In our system, ATG is applied to the interpretation of AFG. Also, ATG is the key component when answering R2 and R4. ATGs in EFI are constructed according to a total of 256 panels covering 12 tactics, 123 techniques and 256 sub-techniques of MITRE ATT&CK.

To evaluate the effectiveness of the ATG, we randomly selected 50 techniques that were evenly distributed across different tactics, then implemented these techniques (atomic tests) on a real system with SPADE [52] to collect low-level system logs. The experimental results show that all entities and dependencies (triples) can be found in the filtered graphs, which illustrates that the constructed ATGs truly represent technique implementations on low-level system logs. The specific implementations and system logs of picked atomic tests can be found in our open-source project.

6.3 RQ2: How to prove the effectiveness of graph alignment plus algorithm?

We need to state that *graph alignment plus algorithm* is not only used for AFG interpretation in the normal use of EFI (see Section 4.3 for details). But we also use this algorithm to evaluate the effectiveness of ASG extraction (R3) and AFG generation (R4) in experiment. Therefore, we evaluate the effectiveness of the algorithm on the calculation of alignment scores as well as on the technique-level interpretation.

Graph alignment score calculation: The fundamental purpose of this algorithm is to quantify the extent to which the graph structure of G_q is present in G_p . While the alignment score exceeds a threshold value we assume that G_p contains G_q . We first randomly selected 10 attack graphs from ASGs and set them as G_p one by one, and performed three kinds of operations on each G_p : random edge addition and deletion, random node addition and deletion, and node addition and deletion consistent with MHES. For each processed G_q , the *graph alignment plus algorithm* was applied separately to calculate the alignment scores between the processed graph G_q and the original graph G_p . The average results are shown in Figure 4. We can find that **the impact of adding or deleting an edge on the graph alignment score is much smaller than that of a node**, the reason is that the core of this algorithm lies in computing the NodeScore to fix the candidate nodes, while the addition and deletion of edges only affects a small portion of the pathway. Moreover, **adding or deleting graph nodes according to MHES has a much smaller impact on the final score than randomly adding or deleting graph nodes**, which is in line with our expectation, since the *graph alignment plus algorithm* avoids false negatives of results by considering equivalent semantics. Finally, we find that **the addition operation has less impact on the score than that of the deletion operation**, which is due to the fact that deleting a graph node destroys a large number of path structures where that node exists, leading to a rapid decrease in PathScore.

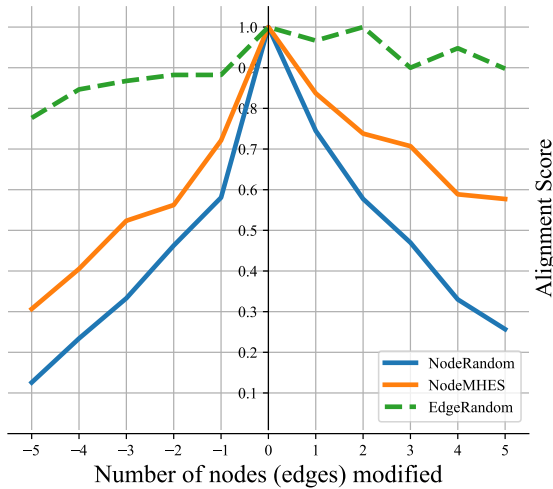


Fig. 4. Change in graph alignment score with graph structure modification. The positive/negative number of the horizontal axis indicates an addition/deletion.

Technique-level interpretation: The *graph alignment plus algorithm* is not only applied to the technique interpretation of AFG in real-world scenarios. Since AFG and ASG

are the same in graph structure and level, here, we used *graph alignment plus algorithm* to identify the ATGs on the manually annotated ASGs (mentioned in Section 6.1) and compared the result with that of latest open-source studies on technique-level interpretation, TTPDrill² and AttackG³, as shown in Table 6. From Table 6, TTPDrill is the worst in terms of overall performance, while EFI is slightly better than AttackG. After analysis, we find that the average number of extracted techniques are 9.9, 17.8 and 7.3 for AttackG, TTPDrill, and EFI, respectively. TTPDrill extracts a large number of techniques because it generates a technique for each sentence without considering contextual information associations. In addition, we find that the precision of AttackG is higher than recall. The reason is that the graph extracted by AttackG is relatively discrete (e.g., the graph is split into five subgraphs on the CTI report “Information gather and exfiltration (TC_A3)” from Darpa TC Dataset, resulting in only one technique being hit). The precision of both TTPDrill and EFI is lower than that of recall (i.e., higher FPs and lower FNs). For TTPDrill, we find that recall is twice as high as precision, the reason is that TTPDrill has an extremely high number of FPs (average 16 FPs per report) and is not interpreted by newer techniques (i.e., new techniques updated by MITRE after 2017). In our design, we prefer to achieve high recall to reduce FNs. Since EFI can dispatch strategies to EDR based on the interpreted results. Even if there are false positives, advance reinforcement will not affect normal operations of the enterprise. However, FNs may cause companies to miss the optimal defence time.

6.4 RQ3: How to prove the effectiveness of ASG extraction?

The purpose of extracting ASGs from CTI reports is to obtain a large number of samples that can be used to train the graph forecast model. **Note that the graph forecast model relies on obtaining information from graph distribution rather than the specific names of entities.** Here, we evaluate the effectiveness of the module in extracting entity attributes, dependency attributes, and overall graph structure, as well as the redundant sentences filtering mentioned in Section 4.1.

Redundant sentences filtering: Since reports from the Darpa TC [48] (TC_A1-A4) are already quite concise (only 6 sentences per report on average), we selected 6 APT organization reports for evaluation. We annotated the attack-relevant sentences as the ground truth by referring to the attack graph drawn in Poirot [37]. Then we input 6 CTI reports into our filtering model (Section 4.1) to get the filtered text. Finally we computed the evaluation metrics on the filtered text and the attack-related sentences, as shown in Table 5. From the table, we can see that the filtering model has a very high performance in terms of recall (i.e., retain attack-related sentences) and a slightly poorer performance in terms of precision (i.e., retain attack-irrelevant sentences). As mentioned in Section 4.3, the number of attack-related sentences in a CTI report is extremely smaller than that of

2. <https://github.com/KaiLiu-Leo/TTPDrill-0.5>

3. <https://github.com/li-zhenyuan/Knowledge-enhanced-Attack-Graph>

TABLE 5

The performance of the model on redundant text filtering. Columns 2 to 4 indicate the number of original text sentences, filtered text sentences, and attack-related sentences, respectively. Column 5 refers to true positive/false positive/true negative/false negative, and columns 6 to 8 refer to the Precision, Recall and F-1 Score calculated with TP/FP/FN.

CTI Reports	Original Text (No. of Sent.)	Filtered Text (No. of Sent.)	Groundtruth Text (No. of Sent.)	TP/FP/FN	Precision (%)	Recall (%)	F1-Score (%)
Carbanak	334	68	49	45/23/3	66.18	91.84	76.93
DeputyDog	65	7	5	5/2/0	71.43	100	83.33
DustySky	297	37	28	26/11/2	70.27	92.86	80.00
njRAT	443	29	24	22/7/2	75.86	91.67	83.02
OceanLotus	199	33	29	24/9/5	72.73	82.76	77.42
Uroburos	154	19	16	16/3/0	84.21	100	91.43
Average	248.5	32.17	25.17	-	73.47	93.19	82.02

attack-unrelated. Therefore, we prefer to reduce false negatives to capture all attack-related sentences in CTI reports. Moreover, after analysis, the poor performance of Carbanak [53] is due to the fact that it contains much descriptive sentences about the characteristics of malicious processes, e.g., ‘Carbanak is a backdoor used by the attackers to compromise the victim’s machine once the exploit, either in the spear phishing email or exploit kit, successfully executes its payload.’

ASG extraction: We evaluated and compared the performance of ASG extraction with the latest open-source studies, AttackG and EXTRACTOR⁴ [16] from three aspects: entities, dependencies, and alignment scores. The evaluation results are shown in Table 6. The left part (columns 5 to 10) reflects the performance of the module on extraction of entity and dependency, and the right part (columns 11 to 14) integrates the performance of the module on extraction of the overall graph structure. From the left part, we find that EFI has an average improvement rate of more than 30% in the three comprehensive evaluation metrics (precision, recall, F-1 Score) compared with the existing work (especially, the improvement rate of recall exceeds 60%), which shows that our EFI is fully ahead of existing work on entity and dependency extraction. In the right part, EFI has an advantage over 200% in the alignment score, which indicates that the ASG extracted by EFI is closer to the ground truth in terms of the overall graph structure. In addition, although the average alignment score of EFI is only 0.593, as shown in Section 6.3, the *graph alignment plus algorithm* is very sensitive to node-level modification, e.g., the alignment score drops to below 0.6 after deleting 2 nodes. And the average number of nodes in our final ASGs is 23 (>2), so **we believe that such deviations do not affect the graph forecast model to learn the information of graph distribution**. Finally, we chose to plot the comparison of three systems and ground truth on TC_A3, as shown in Figure 5. One may argue that the accuracy of extracted ASGs may further affect the prediction model (i.e., potential error propagation will accumulate quickly over the NLP pipeline). It is important to clarify that the role of the ASG extraction module in EFI is to enhance attack samples, with a greater focus on the integrity and rationality of these samples. To address this concern, we have employed the three-stage model from CONAN [10] to validate all ASGs, ensuring their correct attack semantics.

6.5 RQ4: How to prove the effectiveness of AFG generation?

We need to state that, as shown in Section 4.2, the training set of graph forecast model is ASGs (1,429 in total) extracted automatically from CTI reports, and both the input and output of the model are abstract heterogeneous graphs without node names. In order to answer R4, we evaluate the AFG generation of EFI from three aspects: training performance, ASG reconstruction, forecast and interpretation performance and APG reconstruction.

6.5.1 Training Performance

We divided the training set and test set according to the ratio of 8:2 (each ASG is in article level), and recorded metric after each epoch, as shown in Figure 6(a). This sub-graph represents the evaluation performance of the model on the test set. For the specific evaluation metrics we chose the node-level and edge-level loss, as well as the true positive rate (TPR). After more than 40 iterations, **the TPRs of node attributes and edge attributes reach 92% and 73%, respectively**. The main reason why the TPR of edge attributes is lower than that of node is that the adjacency matrix of the graph is sparse (less than 100 non-zero values exist in a 40x40 adjacency matrix), which leads to a sample imbalance problem (the edges with label 0 are much larger than the other edge types, i.e., no such edge exists). We reduced the impact of this problem by limiting the number M of forward prediction, and we set M to 5 and 28 based on the mean and maximum values of the temporal differences between subjects and objects present in all edges within our dataset. We designed control experiments under these two M , as shown in Figure 6. Finally, it can be observed in Figure 6(b) that the node-level loss cannot converge properly, and the edge-level prediction accuracy ends up at only 48%. We believe that the sparsity in the adjacency matrix brings a large impact on the forecast accuracy of edges, and our countermeasure effectively mitigates this problem.

6.5.2 ASG Reconstruction

We apply the graph forecast model to the ASG reconstruction to illustrate the effectiveness of AFG generation (i.e., **simulating the forecast with ASG reconstruction**). The schematic diagram of the experimental procedure is shown in Appendix B. First, we traversed and interpreted all the ASGs (also called original ASG) of test set in technique-level (Figure 9(a), T1566.001, T1204.002, T1574). Second, we deleted nodes (the maximum number of deletion is 5)

4. <https://github.com/ksatvat/EXTRACTOR>

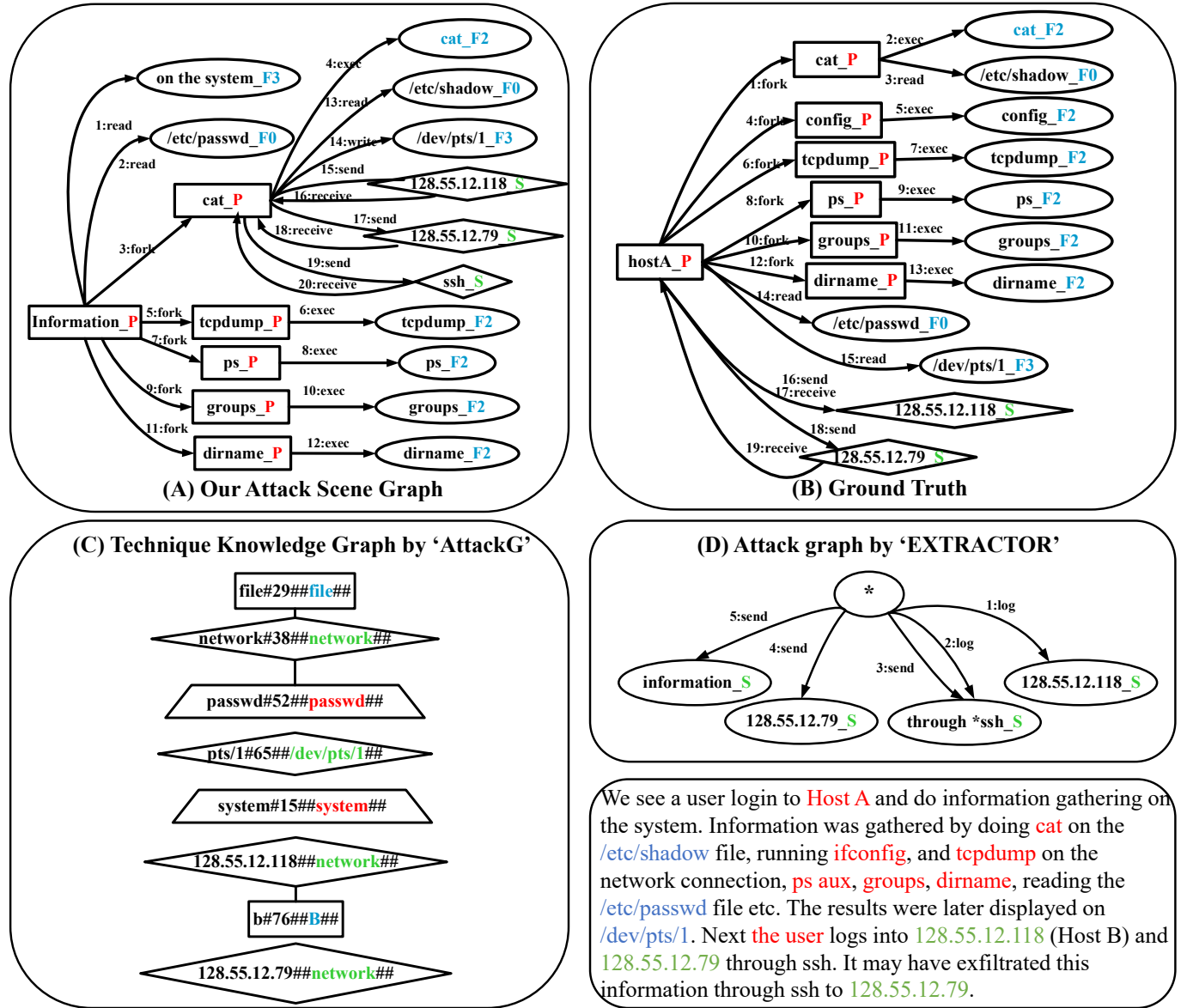


Fig. 5. EFI, AttackG and EXTRACTOR are compared with the extracted ASG using sample TC_Information gather and exfiltration as input, where sub-graph A is our manually extracted Ground Truth. In the figure, red P indicates process, blue F indicates file, and green S indicates socket.

and corresponding edges from the original ASG based on their temporal relevance in a post-order traversal until the deleted subgraph satisfied an ATG, resulting in a broken ASG. We calculated the alignment score between the broken ASG and the original ASG, and recorded the corresponding list of ATGs associated with the broken ASG (Figure 9(b), T1566.001, T1204.002). Then, we input the broken ASG into the trained graph forecast model and generated nodes and edges iteratively until the number of ATGs corresponding to the generated AFG exceeded that of the broken ASG. We refer to this process as **ASG reconstruction**. Finally, we recorded the number of generated nodes and edges, the alignment score of the generated AFG (reconstructed ASG) and the original ASG, and the list of ATGs corresponding to the generated AFG (Figure 9(c), T1566.001, T1204.002, T1574).

After traversing all ASGs of test set, we collected alignment scores under different scenarios as shown in Figure 7(a). We can see that the alignment score between the

broken ASG and the original ASG (blue line in Figure 7(a)) decreases very fast (only 0.067 when $N=5$), which is due to the sensitivity of the *graph alignment plus algorithm* to the node, as shown in Section 6.3. Besides, the average alignment scores of AFG under each number of nodes are much higher than those of broken ASGs (**exceeding 0.27 on average and reaching up to 0.32 when $N=5$**), indicating that graph forecast model can effectively help the broken ASG recover to the original ASG.

6.5.3 APG Reconstruction

In the real scenario, EFI requires APGs provided by EDR tools as input to make forecasts in syslog-level and perform strategy assignment. Therefore, we also tested the effectiveness of EFI for APG reconstruction as a way to verify the effectiveness of EFI for AFG generation in real scenarios. We reproduced DEPIMPACT [49] for correlated sub-graph investigation of alert point, and reproduced DEP-COMM [50] and CPR [51] for compressing redundant edges

TABLE 6

The performance of technique and ASG extracted by different systems in terms of entities, dependencies and alignment score. TC_A1-A4 represent hc attack, ccleaner attack, Information gather and exfiltration, and In-memory attack with firefox in TC report, respectively. The right part (columns 11 to 14) is the alignment score calculated by the *graph alignment plus algorithm*.

CTI Reports	Technique (TP/FP/FN)			Entities (TP/FP/FN)			Dependencies (TP/FP/FN)			Alignment Score		
	AttackG	TTPDrill	EFI	AttackG	Extractor	EFI	AttackG	Extractor	EFI	AttackG	Extractor	EFI
Carbanak	2/10/4	2/24/4	3/3/3	8/13/4	8/14/4	10/4/2	6/12/6	6/20/6	11/12/2	0.248	0.171	0.601
DeputyDog	2/6/3	1/3/4	2/6/3	4/4/2	4/3/2	5/4/1	3/6/2	3/3/2	4/6/1	0.145	0.166	0.687
DustySky	4/5/2	2/17/5	4/5/2	6/7/4	6/4/4	7/6/3	6/8/4	5/3/11	9/10/2	0.118	0.019	0.422
njRAT	4/4/3	1/22/6	4/4/3	8/10/6	6/9/8	10/4/4	7/23/8	5/14/10	12/14/4	0.326	0.241	0.701
OceanLotus	3/2/1	3/44/1	3/6/1	6/11/10	5/6/11	11/6/5	6/11/15	4/11/17	12/9/9	0.361	0.158	0.504
Uroburos	2/22/4	1/12/5	2/1/4	5/6/7	5/5/10	8/5/4	4/7/11	4/3/11	7/8/8	0.137	0.073	0.447
TC_A1	3/0/3	1/10/8	6/4/3	5/3/8	8/11/8	11/3/2	4/4/12	6/7/13	11/14/5	0.212	0.167	0.514
TC_A2	5/11/2	3/7/3	6/3/1	4/1/8	7/10/5	10/7/2	3/3/10	6/6/7	11/8/2	0.085	0.025	0.672
TC_A3	1/0/7	0/6/8	4/6/4	3/5/15	4/5/14	16/2/2	2/3/17	3/4/16	17/6/2	0.167	0.194	0.833
TC_A4	2/10/4	1/16/5	3/2/1	5/4/4	5/10/4	7/4/2	3/5/8	4/8/7	10/9/1	0.249	0.183	0.545
Overall Precision	0.46	0.11	0.51	0.495	0.450	0.668	0.382	0.418	0.513	Overall Alignment Score	0.205	0.140
Overall Recall	0.42	0.23	0.59	0.474	0.478	0.778	0.358	0.350	0.759			
Overall F-1 Score	0.43	0.15	0.53	0.461	0.452	0.715	0.339	0.359	0.605			

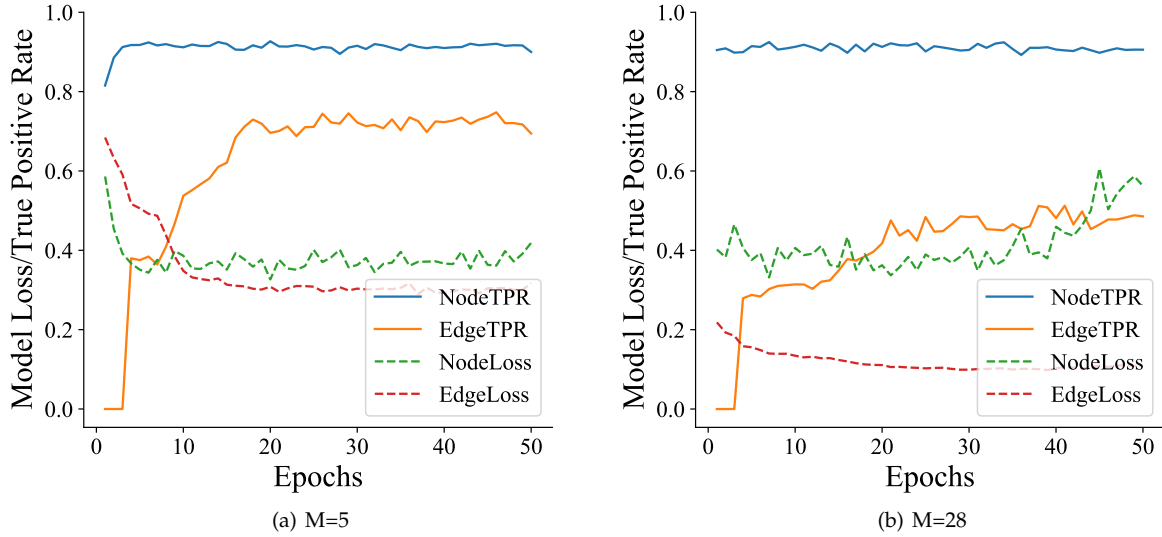


Fig. 6. The performance of forecast model on the test set. The EdgeTPR is calculated by non-zero edges.

and nodes in the sub-graph, to obtain APGs constructed by EDR tools in real scenarios. We chose four attacks (TC_A1-A4) from DARPA Engagement and finally obtained four APGs.

Similar to ASG reconstruction, we started by constructing the broken APG and then proceeded to reconstruct a new AFG. We recorded alignment scores of the broken APG and the generated AFG from the broken APG under different numbers of nodes generation/deletion, as shown in Figure 7(b). First, we can find that the effect of node deletion on APGs is smaller than that on ASGs (shown by the blue line in Figure 7(a) and Figure 7(b)), the reason is that the average number of nodes (18) and edges (21) in the APG is greater than the average number of nodes (11.3) and edges (10.8) in the ASG. In addition, the average alignment score of AFGs are higher than that of the broken APG, exceeding 0.24 on average and 0.27 at maximum. It also indicates that the graph prediction model can effectively assist in recovering the broken APG back to its original state. Due to the intricate structure of the APG, the average increase in alignment score of the reconstructed APG (0.23) is smaller than that of the reconstructed ASG (0.27). However, the goal of EFI is to predict the next move in syslog-level and the alignment score of the reconstructed APG reaches 0.8 when

$N=1$, which indicates that the graph forecast component of EFI will perform well in realistic scenarios in cooperation with EDR tools.

6.5.4 Forecast and Interpretation Performance

In addition to focusing on the evolution of alignment scores, we also make Table 7 to illustrate the forecast performance of EFI in technique-level. From Table 7, we can see that the average deletion of 2.4 nodes decreases the number of ATGs by 4, and the average generation of 1.7 nodes increases the number of ATGs by 3.5. The reason is that it is easy to match multiple ATGs with similar structures after the graph structure is increased.

The metrics in the fifth to seventh rows are calculated using the list of ATGs from original ASG as the ground truth. The broken ASG is obtained by deleting nodes in a post-order traversal of the original ASG, so the list of ATGs from broken ASG must be part of that from original ASG (i.e., precision=1). As we can see, the list of ATGs from AFG performed extremely well on all three metrics, exceeding 90%.

Overhead: Since attackers tend to prioritize lateral movement to the target host or hide themselves after invading the environment. We evaluate the time, CPU and

memory overhead, as well as the real-time requirement for each component of EFI, as shown in Table 8. It can be observed that the average time to extract the ASG is 72.7s and the time to process all CTI reports (3,484) is over 253,000 seconds, but we have no real-time requirement for this component. The average time to generate AFG is less than 4s and the average time to match individual ATG is less than 2s. Even for interpreting a whole AFG, the total time is only 5 mins, which is much less than the average time for lateral movement(1h 58mins) [8]. EFI also has a low overhead in memory (less than 400MB) and CPU (around 15%), and it is entirely possible to reduce the time to process multiple alerts issued by the EDR and explain the whole AFG by multi-processes.

TABLE 7

Results of graph forecast and interpretation. Rows 2-4 are the average number of nodes, edges and technique templates, and rows 5-7 are the precision/recall/F-1 score obtained by calculating the TP/FP/FN using the ATGs corresponding to original ASG as the ground truth.

	Original ASG	Broken ASG	AFG
Node	11.3	8.9	10.6
Edge	10.8	8.1	9.9
The number of ATGs	13.5	9.5	13
Overall Precision	1	1	0.918
Overall Recall	1	0.641	0.903
Overall F1-score	1	0.717	0.906

7 DISCUSSION AND LIMITATION

ASG extraction: Regarding the automatic extraction of ASGs from the CTI reports, as shown in Table 6, we notice that there are several FPs and FNs. The reason is that CTI reports combine two features: natural language complexity and prominent domain features. Fortunately, our graph forecast model is based on graph distribution rather than graph details. In addition, we abstract the nodes to further weaken the impact of less-than-perfect ASG extraction on model training. In the future, we can perform text clustering and template extraction on CTI reports to generate more accurate ASGs.

ATG and graph forecast model: Due to the nature of the atomic technique, the average number of nodes and edges per ATG is small (only 5.1 nodes and 4.7 edges), which leads to some FPs when using a ATG to interpret a AFG. In the future, we will also try to subdivide node and edge attributes (e.g., subdividing the registry into HKC, HKLM, and HKU) to mitigate the problem. While for the graph forecast model, it can't generate a AFG with the number of matching ATGs plus one within a predetermined M steps (M=5) for some inputs. We consider that these inputs already have a complete structure on attack graph and thus cannot continue to be predicted.

8 RELATED WORK

Information extraction from CTI: CTI plays an important role in security confrontations [7, 54]. The data shared by these open source platforms, while structured and machine-readable, is single-point independent and lacks information

about interactions with other IOCs, which leads to the inability of vendors to capture complete attacks.

Recently researchers have attempted to automate the extraction of information from unstructured CTI reports. iACE [55] proposes a graph mining technique to collect IOCs from CTI reports, improving the recognition rate of IOCs and NERs, but still missing the classification of inter-entity dependencies. TTPDrill [15] uses a dependency interpreter to extract binary groups (verbs, objects) from each sentence and determine the attack technique corresponding to this sentence by calculating the similarity. However, this work does not analyze the contextual information of the sentence, while relying extremely on the benchmark dataset (called Ontology in its work). ChainSmith [56] extracts IOCs using regular expressions and maps them to a certain campaign phase using a classifier. However, they ignore the relationship between IOCs and do not consider other attack-related entities (as shown in Section 4.1) that play an important role in CTI reports. EXTRACTOR [16] and ThreatRaptor [54] extract information from CTI reports through a custom NLP pipeline, but both suffer from certain problems. EXTRACTOR classifies all IOC-free entities as the same malicious entity, resulting in a star-shaped structure of the generated graph while ignoring the case where the attacker uses multiple malicious processes to reach one target. ThreatRaptor extracts relationships between IOCs to build the traceability graph, but ignores common co-reference cases in CTI reports. AttackG [17] tends to extract the Technique Knowledge Graph, but it lacks information extraction of specific types of dependencies between entities and does not perform text redundancy filtering, which lead to the generation of many separate sub-graphs. Unlike previous work, the ASG extracted by EFI is a holistic heterogeneous graph with node and dependency attributes that can be mapped to the low-level system logs.

Technique-level interpretation: With the increasing usage of system logs for causal analysis and multi-stage attack detection [57–59], analysts have found a huge semantic gap between the low-level system logs and the high-level techniques, i.e., a large combination of low-level logs is required to reflect the high-level technique. Therefore, Analysts attempt to combine provenance graph with ATT&CK to map low-level system logs to high-level attackers' technique aid in a comprehensive analysis. Both HOLMES [7] and RapSheet [22] design detection rules by observing how the technique is implemented and determine the technique stage corresponding to the alert stage. However, they both rely entirely on manual policies, making it difficult to identify novel attack techniques. To interpret the attack graphs extracted from CTI reports in technique-level, Poirot [37] designed a graph alignment algorithm that predetermines candidate nodes and calculates contribution scores separately to fix structure to find possible attack graphs embedded in provenance graph. However, the extraction of attack graphs is manual and does not consider the multi-hop equivalent semantic case which is common in attacks. AttackG [17] implements the automatic extraction of technique templates and attack graphs, and interprets the attack graphs at a technique-level. However, technical templates and attack graphs generated by AttackG are discrete, leading further generalized impossible. In addition, AttackG focuses too

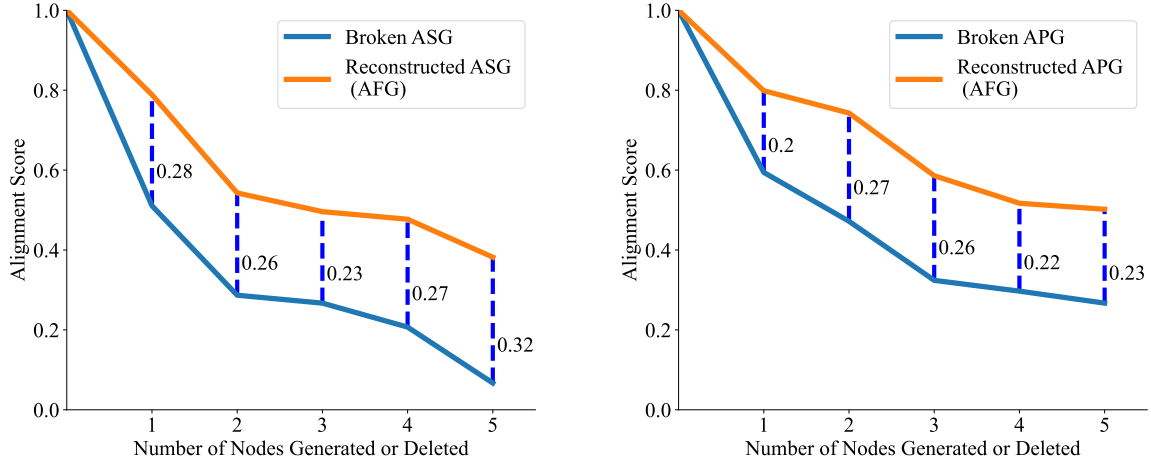


Fig. 7. Change in graph alignment score with graph structure modification. The horizontal coordinate value is the number of node deletions for broken ASG/APG and the number of node generation for AFG. The vertical dashed line indicates the difference in graph alignment score between the broken graph and the AFG.

TABLE 8

The overhead and real-time requirements of the EFI component. The second column is the overhead of extracting ASG, the third column is the overhead of generating AFG, the fourth column is the overhead of investigating APG (from [49, 50]), the fifth column is the overhead of computing individual ATG alignment scores, and the sixth column is the overhead of interpreting a whole AFG.

Overhead	ASG Extraction	AFG Generation	APG Investigation	One ATG Match	Whole AFG Interpretation
Time	72.7s	3.6s	314.8s	1.9s	307.9s
CPU	11.2%	7.1%	14.9%	6.5%	6.7%
Real-time Requirement	No	Yes	Yes	Yes	Yes
Memories	337.4MB	281.1MB	376.0MB	169.7MB	170.1MB

much on the names of entities and leads to a poor graph alignment score. On the contrary, we combine elaborate ATGs and *graph alignment plus algorithm*, consider abstract nodes and multi-hop semantic equivalence cases, to interpret AFG and minimize false negatives.

Generation algorithms and models: There have been a number of studies on deep learning generative models, but all of them have certain problems. For example, VGAE [60] and Graphite [61] propose graph generation models based on variational autocoders, but they are limited to learning from a single graph. GraphVAE [62] propose a VAE-based approach to generate graphs, while it only can generate small graphs with less than 40 nodes. In addition, GraphRNN [36] proposes a neural network for sequentially generating graph to satisfy the requirement of large graphs, but it only considered isomorphic graphs. Both Tiresias [63] and DEEPCASE [64] utilize the alert sequences of EDR and combine them with a neural network to predict the next alert. However, their predictive capabilities are limited to EDR (Symantec) alert levels for non-graphical data structures, thus lacking universality. Unlike previous work, EFI's graph forecast model can automatically learn graph distributions from massive sample graphs and generate heterogeneous graphs with node attributes and dependency attributes of arbitrary size.

9 CONCLUSION

In this paper, we propose a real-time post-exploitation attack forecasting and interpreting system, EFI. It can get one step ahead of the attacker, automatically predict next move during post-exploitation, explain attacks in technique-level and dispatch strategies to EDR for advance reinforcement. It also can avoid the impact of existing EDR false positives, and reduce the attack surface of system without affecting the normal operations. Experiments show that the forecast and interpretation precision of EFI can reach 91.8%. To the best of our knowledge, we are the first to work on automated forecasting and interpreting post-exploitation attacks in syslog-level.

REFERENCES

- [1] CSIS, "Significant cyber incidents," 2023, <https://www.csis.org/programs/strategic-technologies-program/significant-cyber-incidents/>. [Online]. Available: <https://www.csis.org/programs/strategic-technologies-program/significant-cyber-incidents>
- [2] "Windows event tracing," <https://docs.microsoft.com/en-us/windows/desktop/ETW/event-tracing-portal/>. [Online]. Available: <https://docs.microsoft.com/en-us/windows/desktop/ETW/event-tracing-portal>
- [3] "The linux audit daemon," <https://linux.die.net/man/8/auditd/>. [Online]. Available: <https://linux.die.net/man/8/auditd>

- [4] T. Zhu, J. Wang, L. Ruan, C. Xiong, J. Yu, Y. Li, Y. Chen, M. Lv, and T. Chen, "General, efficient, and real-time data compaction strategy for apt forensic analysis," *IEEE Transactions on Information Forensics and Security*, vol. 16, pp. 3312–3325, 2021.
- [5] M. N. Hossain, S. M. Milajerdi, J. Wang, B. Eshete, R. Gjomemo, R. Sekar, S. Stoller, and V. Venkatakrishnan, "{SLEUTH}: Real-time attack scenario reconstruction from {COTS} audit data," in *USENIX Security Symposium*, 2017, pp. 487–504.
- [6] "Mitre att&ck," <https://attack.mitre.org/>. [Online]. Available: <https://attack.mitre.org>
- [7] S. M. Milajerdi, R. Gjomemo, B. Eshete, R. Sekar, and V. Venkatakrishnan, "Holmes: real-time apt detection through correlation of suspicious information flows," in *2019 IEEE Symposium on Security and Privacy (SP)*. IEEE, 2019, pp. 1137–1152.
- [8] CrowdStrike, "Lateral movement," 2022, <https://www.crowdstrike.com/cybersecurity-101/lateral-movement/>.
- [9] W. U. Hassan, S. Guo, D. Li, Z. Chen, K. Jee, Z. Li, and A. Bates, "Nodoze: Combatting threat alert fatigue with automated provenance triage," in *network and distributed systems security symposium*, 2019.
- [10] C. Xiong, T. Zhu, W. Dong, L. Ruan, R. Yang, Y. Chen, Y. Cheng, S. Cheng, and X. Chen, "Conan: A practical real-time apt detection system with high accuracy and efficiency," *IEEE Transactions on Dependable and Secure Computing*, 2020.
- [11] M. N. Hossain, S. Sheikhi, and R. Sekar, "Combating dependence explosion in forensic analysis using alternative tag propagation semantics," in *2020 IEEE Symposium on Security and Privacy (SP)*. IEEE, 2020, pp. 1139–1155.
- [12] F. Liu, Y. Wen, D. Zhang, X. Jiang, X. Xing, and D. Meng, "Log2vec: A heterogeneous graph embedding based approach for detecting cyber threats within enterprise," in *Proceedings of the 2019 ACM SIGSAC Conference on Computer and Communications Security*, 2019, pp. 1777–1794.
- [13] X. Han, T. Pasquier, A. Bates, J. Mickens, and M. Seltzer, "Unicorn: Runtime provenance-based detector for advanced persistent threats," *arXiv preprint arXiv:2001.01525*, 2020.
- [14] T. Chen, C. Dong, M. Lv, Q. Song, H. Liu, T. Zhu, K. Xu, L. Chen, S. Ji, and Y. Fan, "Apt-kgl: An intelligent apt detection system based on threat knowledge and heterogeneous provenance graph learning," *IEEE Transactions on Dependable and Secure Computing*, 2022.
- [15] G. Husari, E. Al-Shaer, M. Ahmed, B. Chu, and X. Niu, "Ttpdrill: Automatic and accurate extraction of threat actions from unstructured text of cti sources," in *Proceedings of the 33rd annual computer security applications conference*, 2017, pp. 103–115.
- [16] K. Satvat, R. Gjomemo, and V. Venkatakrishnan, "Extractor: Extracting attack behavior from threat reports," in *2021 IEEE European Symposium on Security and Privacy (EuroS&P)*. IEEE, 2021, pp. 598–615.
- [17] Z. Li, J. Zeng, Y. Chen, and Z. Liang, "Attackg: Constructing technique knowledge graph from cyber threat intelligence reports," *arXiv preprint arXiv:2111.07093*, 2021.
- [18] "Meet the atomic family — atomic red team," <https://atomicredteam.io/>.
- [19] "Russia's fancy bear hackers likely penetrated a us federal agency," <https://www.wired.com/story/russias-fancy-bear-hack-us-federal-agency/>. [Online]. Available: <https://www.wired.com/story/russias-fancy-bear-hack-us-federal-agency/>
- [20] "Apt 28," <https://attack.mitre.org/groups/G0007/>. [Online]. Available: <https://attack.mitre.org/groups/G0007/>
- [21] "Endpoint detection and response solutions market," <https://www.gartner.com/reviews/market/endpoint-detection-and-response-solutions/>. [Online]. Available: <https://www.gartner.com/reviews/market/endpoint-detection-and-response-solutions>
- [22] W. U. Hassan, A. Bates, and D. Marino, "Tactical provenance analysis for endpoint detection and response systems," in *2020 IEEE Symposium on Security and Privacy (SP)*. IEEE, 2020, pp. 1172–1189.
- [23] W. U. Hassan, M. A. Nouredine, P. Datta, and A. Bates, "Omegalog: High-fidelity attack investigation via transparent multi-layer log analysis," in *Network and distributed system security symposium*, 2020.
- [24] T. Zhu, J. Yu, C. Xiong, W. Cheng, Q. Yuan, J. Ying, T. Chen, J. Zhang, M. Lv, Y. Chen *et al.*, "Aptshield: A stable, efficient and real-time apt detection system for linux hosts," *IEEE Transactions on Dependable and Secure Computing*, 2023.
- [25] "3rd update: Cyber espionage reaches new levels with flamer," <https://www.bitdefender.com/blog/labs/cyber-espionage-reaches-new-levels-with-flamer/>. [Online]. Available: <https://www.bitdefender.com/blog/labs/cyber-espionage-reaches-new-levels-with-flamer/>
- [26] J. Devlin, M.-W. Chang, K. Lee, and K. Toutanova, "Bert: Pre-training of deep bidirectional transformers for language understanding," *arXiv preprint arXiv:1810.04805*, 2018.
- [27] Z. Huang, W. Xu, and K. Yu, "Bidirectional lstm-crf models for sequence tagging," *arXiv preprint arXiv:1508.01991*, 2015.
- [28] A. Radford and K. Narasimhan, "Improving language understanding by generative pre-training," 2018. [Online]. Available: <https://api.semanticscholar.org/CorpusID:49313245>
- [29] G. Lample, M. Ballesteros, S. Subramanian, K. Kawakami, and C. Dyer, "Neural architectures for named entity recognition," *arXiv preprint arXiv:1603.01360*, 2016.
- [30] A. Graves, A.-r. Mohamed, and G. Hinton, "Speech recognition with deep recurrent neural networks," in *2013 IEEE international conference on acoustics, speech and signal processing*. Ieee, 2013, pp. 6645–6649.
- [31] J. D. Lafferty, A. McCallum, and F. Pereira, "Conditional random fields: Probabilistic models for segmenting and labeling sequence data," in *International Conference on Machine Learning*, 2001. [Online]. Available: <https://api.semanticscholar.org/CorpusID:219683473>
- [32] "Neuralcoref 4.0: Coreference resolution in spacy with neural networks," 2020, <https://github.com/>

- huggingface/neuralcoref/.
- [33] E. Brill, "A simple rule-based part of speech tagger," Pennsylvania Univ Philadelphia Dept of Computer and Information Science, Tech. Rep., 1992.
 - [34] A. Culotta and J. Sorensen, "Dependency tree kernels for relation extraction," in *Proceedings of the 42nd annual meeting of the association for computational linguistics (ACL-04)*, 2004, pp. 423–429.
 - [35] T. Mikolov, K. Chen, G. Corrado, and J. Dean, "Efficient estimation of word representations in vector space," *arXiv preprint arXiv:1301.3781*, 2013.
 - [36] J. You, R. Ying, X. Ren, W. Hamilton, and J. Leskovec, "Graphrnn: Generating realistic graphs with deep autoregressive models," in *International conference on machine learning*. PMLR, 2018, pp. 5708–5717.
 - [37] S. M. Milajerdi, B. Eshete, R. Gjomemo, and V. Venkatakrishnan, "Poirot: Aligning attack behavior with kernel audit records for cyber threat hunting," in *Proceedings of the 2019 ACM SIGSAC conference on computer and communications security*, 2019, pp. 1795–1812.
 - [38] E. Loper and S. Bird, "Nltk: the natural language toolkit," <https://pyod.readthedocs.io/en/latest/>.
 - [39] "spacy-industrial-strength natural language processing," 2020, <https://spacy.io/>.
 - [40] "Bitdefenderblog," <https://www.bitdefender.com/blog/>.
 - [41] "Microsoft security-intelligence," <https://www.microsoft.com/security/blog/security-intelligence/>. [Online]. Available: <https://www.microsoft.com/security/blog/security-intelligence/>
 - [42] "Broadcom software blogs," <https://symantec-enterprise-blogs.security.com/blogs/>. [Online]. Available: <https://symantec-enterprise-blogs.security.com/blogs/>
 - [43] "Talos blog," <https://blog.talosintelligence.com/>. [Online]. Available: <https://blog.talosintelligence.com/>
 - [44] "Virusotalblog," <https://www.blog.virustotal.com/>.
 - [45] L. A. Ramshaw and M. P. Marcus, "Text chunking using transformation-based learning," *Natural language processing using very large corpora*, pp. 157–176, 1999.
 - [46] "Graphviz," <https://graphviz.org/>.
 - [47] "Networkx," <https://networkx.org/>.
 - [48] "Darpa transparent computing engagement," 2020, <https://www.darpa.mil/program/transparent-computing>.
 - [49] P. Fang, P. Gao, C. Liu, E. Ayday, K. Jee, T. Wang, Y. F. Ye, Z. Liu, and X. Xiao, "{Back-Propagating} system dependency impact for attack investigation," in *31st USENIX Security Symposium (USENIX Security 22)*, 2022, pp. 2461–2478.
 - [50] Z. Xu, P. Fang, C. Liu, X. Xiao, Y. Wen, and D. Meng, "Depcomm: Graph summarization on system audit logs for attack investigation," in *2022 IEEE Symposium on Security and Privacy (SP)*. IEEE, 2022, pp. 540–557.
 - [51] Z. Xu, Z. Wu, Z. Li, K. Jee, J. Rhee, X. Xiao, F. Xu, H. Wang, and G. Jiang, "High fidelity data reduction for big data security dependency analyses," in *Proceedings of the 2016 ACM SIGSAC conference on computer and communications security*, 2016, pp. 504–516.
 - [52] "Spade," <https://github.com/ashish-gehani/SPADE>.
 - [53] K. L. G. R. . A. T. (GReAT), "Carbanak apt: The great bank robbery." 2015, https://media.kasperskycontenthub.com/wp-content/uploads/sites/43/2018/03/08064518/Carbanak_APT_eng.pdf.
 - [54] P. Gao, F. Shao, X. Liu, X. Xiao, Z. Qin, F. Xu, P. Mittal, S. R. Kulkarni, and D. Song, "Enabling efficient cyber threat hunting with cyber threat intelligence," in *2021 IEEE 37th International Conference on Data Engineering (ICDE)*. IEEE, 2021, pp. 193–204.
 - [55] X. Liao, K. Yuan, X. Wang, Z. Li, L. Xing, and R. Beyah, "Acing the ioc game: Toward automatic discovery and analysis of open-source cyber threat intelligence," in *Proceedings of the 2016 ACM SIGSAC conference on computer and communications security*, 2016, pp. 755–766.
 - [56] Z. Zhu and T. Dumitras, "Chainsmith: Automatically learning the semantics of malicious campaigns by mining threat intelligence reports," in *2018 IEEE European symposium on security and privacy (EuroS&P)*. IEEE, 2018, pp. 458–472.
 - [57] A. Bates, D. J. Tian, K. R. Butler, and T. Moyer, "Trustworthy {Whole-System} provenance for the linux kernel," in *24th USENIX Security Symposium (USENIX Security 15)*, 2015, pp. 319–334.
 - [58] S. T. King and P. M. Chen, "Backtracking intrusions," in *Proceedings of the nineteenth ACM symposium on Operating systems principles*, 2003, pp. 223–236.
 - [59] D. J. Pohly, S. McLaughlin, P. McDaniel, and K. Butler, "Hi-fi: collecting high-fidelity whole-system provenance," in *Proceedings of the 28th Annual Computer Security Applications Conference*, 2012, pp. 259–268.
 - [60] T. N. Kipf and M. Welling, "Variational graph auto-encoders," *arXiv preprint arXiv:1611.07308*, 2016.
 - [61] A. Grover, A. Zweig, and S. Ermon, "Graphite: Iterative generative modeling of graphs," in *International conference on machine learning*. PMLR, 2019, pp. 2434–2444.
 - [62] M. Simonovsky and N. Komodakis, "Graphvae: Towards generation of small graphs using variational autoencoders," in *International conference on artificial neural networks*. Springer, 2018, pp. 412–422.
 - [63] Y. Shen, E. Mariconti, P. A. Vervier, and G. Stringhini, "Tiresias: Predicting security events through deep learning," in *Proceedings of the 2018 ACM SIGSAC Conference on Computer and Communications Security*, 2018, pp. 592–605.
 - [64] T. van Ede, H. Aghakhani, N. Spahn, R. Bortolameotti, M. Cova, A. Continella, M. van Steen, A. Peter, C. Kruegel, and G. Vigna, "Deepcase: Semi-supervised contextual analysis of security events," *IEEE Security and Privacy*, 2022.

APPENDIX A

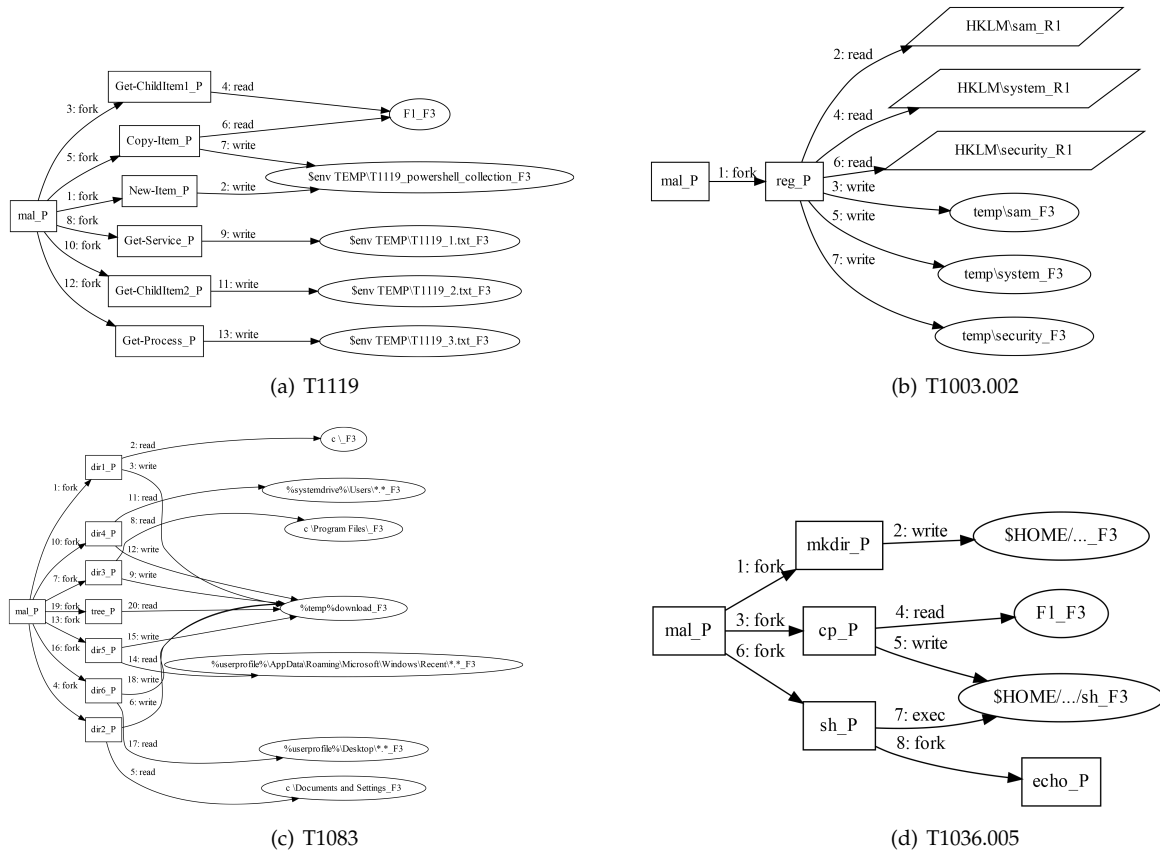
ATG EXAMPLES

We manually constructed the ATG for each atomic test by reviewing the descriptions of all the atomic red team techniques and the command lines of the test cases. As shown in Figure 8, we show 4 ATGs along with a brief description of the technique goals.

APPENDIX B

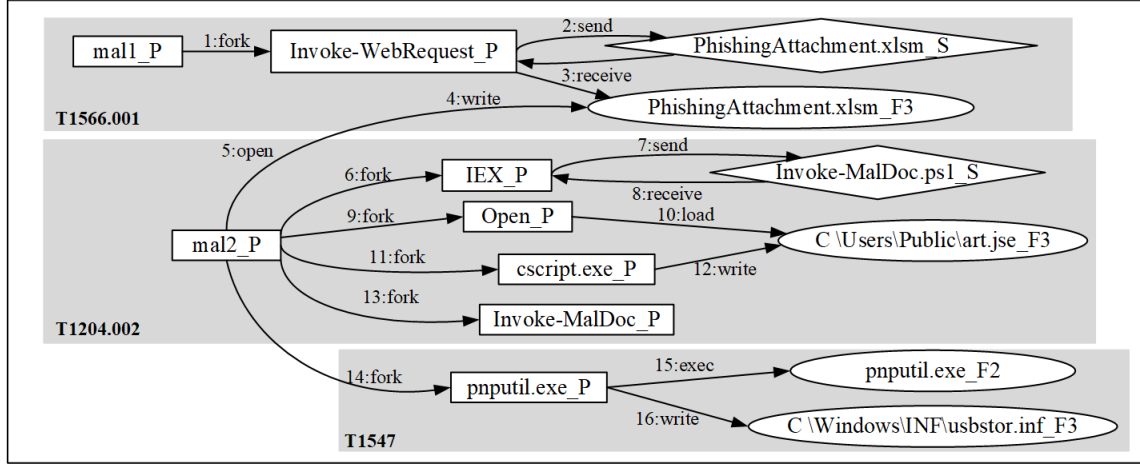
APPROACH OF EVALUATING GRAPH FORECAST MODEL

As described in Section 6.5 and Figure 9, we designed an experimental approach to evaluate the effectiveness of the graph prediction model. The red dashed line indicates the removed nodes and dependencies, the blue dashed line indicates the forecast nodes and dependencies, and the shading indicates the technique-level interpretation. The technique-level interpretation results for the original ASG (sub-graph A) are: T1566.001, T1204.002, T1574, for the broken ASG (sub-graph B) are: T1566.001, T1204.002, for the AFG (sub-graph C) are: T1566.001, T1204.002, T1574.

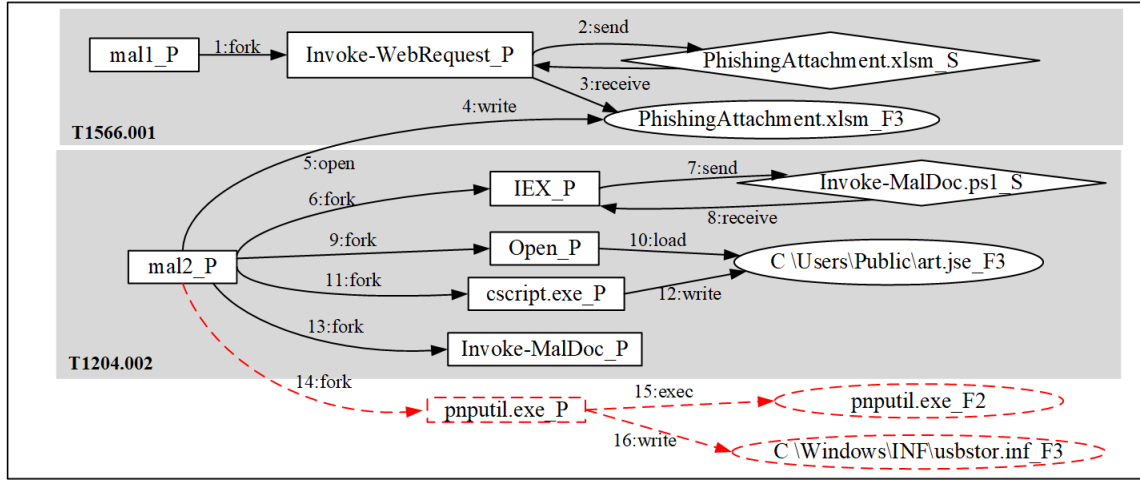


- (A) Adversary may use automated techniques for collecting internal data, such as file type, location, or name at specific time intervals.
- (B) Adversaries may extract credential material from the SAM database, which contains local accounts for the host.
- (C) Adversaries may search files and directories for certain information within a file system to shape follow-on behaviors.
- (D) Adversaries may match or approximate the name or location of legitimate files when naming/placing them, for the sake of evading defenses and observation.

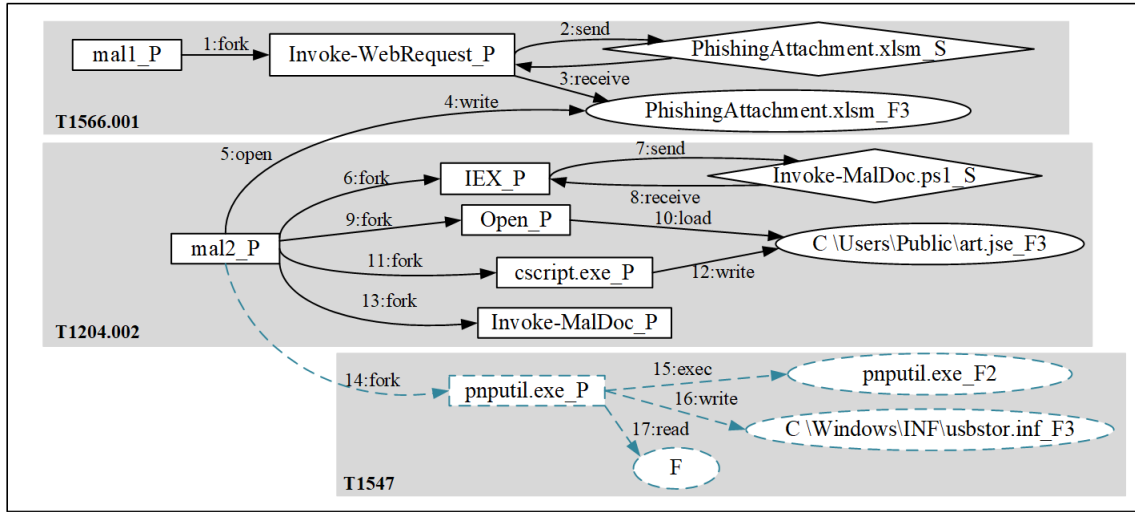
Fig. 8. The examples of manually constructed ATG.



(a) Original ASG



(b) Broken ASG



(c) AFG

Fig. 9. The experimental results of graph forecast and interpretation. Figure 9(a) indicates the original ASG, Figure 9(b) indicates the broken ASG, and Figure 9(c) indicates the AFG. The red dashed line indicates the removed nodes and dependencies, the blue dashed line indicates the forecast nodes and dependencies, and the dash area indicates the technique-level interpretation.